Mineralogical Magazine (2023), **87**, 645–658
doi:10.1180/mgm.2023.32

CAMBRIDGE UNIVERSITY PRESS

Article

Crystallisation of Ca-bearing nepheline in basanites from Kajishiyama, Tsuyama Basin, Southwest Japan

Keiya Yoneoka[1,2], Maki Hamada[3] and Shoji Arai[3]

[1]Graduate school of Natural Science and Technology, Kanazawa University, Kanazawa, 920-1192, Japan; [2] Research Institute of Geology and Geoinformation, Geological Survey of Japan, National Institute of Advanced Industrial Science and Technology (AIST), Tsukuba, 305-8567, Japan; and [3] School of Geoscience and Civil Engineering, College of Science and Engineering, Kanazawa University, Kanazawa, 920-1192, Japan

Abstract

Ca-bearing nepheline found in the Kajishiyama basanite, Tsuyama Basin, southwest Japan, was investigated to clarify its genesis in silica-undersaturated magmas. The basanite contains olivine and augite as phenocrysts and microphenocrysts, with Ca-bearing nepheline, olivine, augite, ulvöspinel, plagioclase, alkali feldspar, apatite and zeolites in the groundmass. Zeolites are more abundant in coarser-grained samples. The whole-rock composition of the basanite is characterised by low SiO_2 and P_2O_5 contents and high total Fe, MgO, Na_2O, K_2O, Ba and Sr contents.

The Ca-bearing nepheline, ~20 μm in size, occurs in the mesostasis of the Kajishiyama basanite and contains up to 2.31 wt.% CaO and 16.75 wt.% Na_2O, in contrast to nepheline from the Hamada nephelinite, southwest Japan. The approximate compositional formula of the Kajishiyama nepheline with the highest Ca content is $(Ca_{0.467}Ba_{0.013}Na_{5.286}K_{0.919}\square^{Total}_{1.385})_{\Sigma 8.070}(Si_{0.912}Al_{6.980}Cr^{3+}_{0.003}Fe^{3+}_{0.067}Mg_{0.017})_{\Sigma 7.979}Si_{8.000}O_{32}$; i.e. $Ne_{65.50}Ks_{11.39}Q^{xs}_{11.22}CaNe_{11.89}$.

Basanites are defined as being nepheline-normative, however they are high in normative plagioclase, the amount of which increases with fractionation of the magma. Nepheline crystallised after plagioclase, at the last stage of magmatic solidification is enriched in Ca. Such Ca-rich nepheline only forms from a magma which is high in normative plagioclase, as is the case in the Kajishiyama basanite. In contrast, Ca-poor nepheline is precipitated from nephelinitic magmas that crystallise melilite instead of plagioclase, even when Ca contents are high.

Keywords: Ca-rich nepheline; melilite; basanite; nephelinite; Tsuyama Basin; silica-undersaturated mafic magma

(Received 14 July 2022; accepted 24 April 2023; Accepted Manuscript published online: 2 May 2023; Associate Editor: Ian Coulson)

Introduction

Nepheline is a feldspathoid mineral with an ideal formula of $K_2Na_6Al_8Si_8O_{32}$ ($Z = 1$) (Donnay *et al.*, 1959; Hamada *et al.*, 2019) and is a typical rock-forming mineral in terrestrial silica-undersaturated alkaline rocks (Deer *et al.*, 1963). It has also been reported in extra-terrestrial materials such as carbonaceous chondrites (Allen *et al.*, 1970; Kimura and Ikeda, 1995) and ordinary chondrites (Ikeda, 1980).

Nepheline is classified as a tectosilicate and has a framework structure of four crystallographically independent tetrahedral sites. The general structural formula is $A_2B_6T1_4T2_4T3_4T4_4O_{32}$ ($Z = 1$), where the *T*1 and *T*2 sites are one set of tetrahedral sites residing on special equivalent positions along the [001] triads forming distorted oval ring channels (labelled as *B* channel). The *T*3 and *T*4 sites of the second set of tetrahedral sites lie on general equivalent positions along the [001] triads and form hexagonal ring channels (designated as *A* channel) (Hahn and Buerger, 1955). The *T*1 and *T*4 sites are mainly occupied by Al^{3+}, whereas the *T*2 and *T*3 sites are mainly occupied by Si^{4+}, and for this 'ideal' composition K^+ and Na^+ are distributed in the *A* and *B* channels, respectively (Hahn and Buerger, 1955; Foreman and Peacor, 1970; Dollase, 1970; Simmons and Peacor, 1972; Vulić *et al.*, 2011; Balassone *et al.*, 2014; Hamada *et al.*, 2019). Thus, the Na to K ratio of ideal nepheline is 3:1, though almost all natural nephelines depart from this ratio due to substitutions, such as: (1) $K^+ + Al^{3+} \rightarrow \square + Si^{4+}$, where $\square$ is a vacancy in site *A*; (2) replacement of K^+ with Na^+ at the *A* site (Dollase and Thomas, 1978); and (3) replacement of Na^+ with K^+ at the *B* site (Hamada *et al.*, 2019). In addition, other cations, discussed below, are known to cause nepheline compositional variations. Henderson (2020) concluded that Mg^{2+}, Mn^{2+} and Ti^{4+} replace Si^{4+} in the tetrahedral site, and large cations such as Ca^{2+}, Ba^{2+} and Sr^{2+} replace Na^+ and K^+ in the cavity sites and suggested a method to calculate the molecular nepheline formula. Henderson and Oliveira (2022) modified that calculation method in order to deal with the presence of Fe^{2+}, Mg^{2+} and Mn^{2+} in tetrahedral sites, and Oliveira and Henderson (2022) proposed a method to estimate Fe^{2+} occurrence in nepheline. However, the content and site occupancies of minor and trace elements such as Ca^{2+}, Mg^{2+}, Mn^{2+}, Fe^{2+} and Ti^{4+} in nepheline have not been

Corresponding author: Keiya Yoneoka; Email: k.yoneoka@aist.go.jp Maki Hamada; Email: hamada-m@se.kanazawa-u.ac.jp

Cite this article: Yoneoka K., Hamada M. and Arai S. (2023) Crystallisation of Ca-bearing nepheline in basanites from Kajishiyama, Tsuyama Basin, Southwest Japan. *Mineralogical Magazine* **87**, 645–658. https://doi.org/10.1180/mgm.2023.32

studied systematically due to rather limited occurrences of nepheline and the difficulty of preparation of nepheline crystals suitable for detailed structural investigations. Therefore, further studies on the occurrence, composition, intra-crystalline distributions of cations, and structural properties of minor element-bearing nephelines are required.

Ca-bearing nephelines have been reported from silica-undersaturated igneous rocks such as basanite from the Korath range, Ethiopia (Brown and Carmichael, 1969); pulaskite (nepheline–plagioclase syenite) from the Marangudzi complex, Zimbabwe (Henderson and Gibb, 1972); and basanites from Nanzaki (Fig. 1) (Goto and Arai, 1986; Oshika *et al.*, 2014) and Kajishiyama (Hirai and Arai, 1986) in Japan. However, their detailed compositional characteristics and formation processes were not examined thoroughly in those studies. In addition, nepheline from the Hamada nephelinite, southwest Japan, is Ca-poor, although it shares a similar age and tectonic setting of eruption with the Kajishiyama basanite (Fig. 1) (Kimura *et al.*, 2005a; Nguyen *et al.*, 2020). In this investigation we describe the Ca-bearing nepheline and associated minerals in the Kajishiyama basanite in more detail and discuss the genesis of Ca-bearing nepheline in comparison with Ca-poor varieties from other nephelinites.

Geological background

In the Japan arc terrains, alkaline basalts, and especially basanites and nephelinites, have been reported primarily in the Japan Sea side of the Chugoku district (Fig. 1) (Takamura, 1973; Nakamura *et al.*, 1986; Iwamori, 1991; Tatsumi *et al.*, 1999; Hamada, 2011; Hamada *et al.*, 2019).

Kajishiyama (35°02′55.7″N, 133°50′05.0″E) is located in the Tsuyama Basin, where there occurs monogenetic volcanoes of alkaline basalts with Ca-bearing nepheline (Hirai and Arai, 1983, 1986). The Kajishiyama basanite, located ~15 km west of Tsuyama in the Okayama Prefecture, Japan, originally formed a small volcanic dome on the basement of the Sangun metamorphic rocks (Takamura, 1973; Fig. 1). The dome has been highly dissected, and we collected representative samples from loose blocks near the summit of the residual hill (Hirai and Arai, 1983). Uto *et al.* (1986) reported a K–Ar radiometric age of 6.5±0.3 Ma for the Kajishiyama basanite. Takamura (1973) determined the whole-rock composition of the basanite, showing that it is highly silica-undersaturated, containing 40.94 wt.% SiO_2 and 20.39 wt.% normative nepheline. Modal nepheline was first recognised in this basanite by Hirai and Arai (1983), who discussed the temperature and stages of crystallisation of nepheline and feldspar on the basis of their compositions. In addition, Hirai and Arai (1986) showed that there is a relationship between the modal amounts of nepheline, feldspars and zeolites in the Noyamadake basanite, and suggested the reaction "Nepheline + Feldspars + H_2O → Zeolites" occurred during the deuteric alteration of the solidified basanite.

Petrography

The Kajishiyama basanites are massive, dark grey, and vary in grain size from fine to relatively coarse grained. Samples

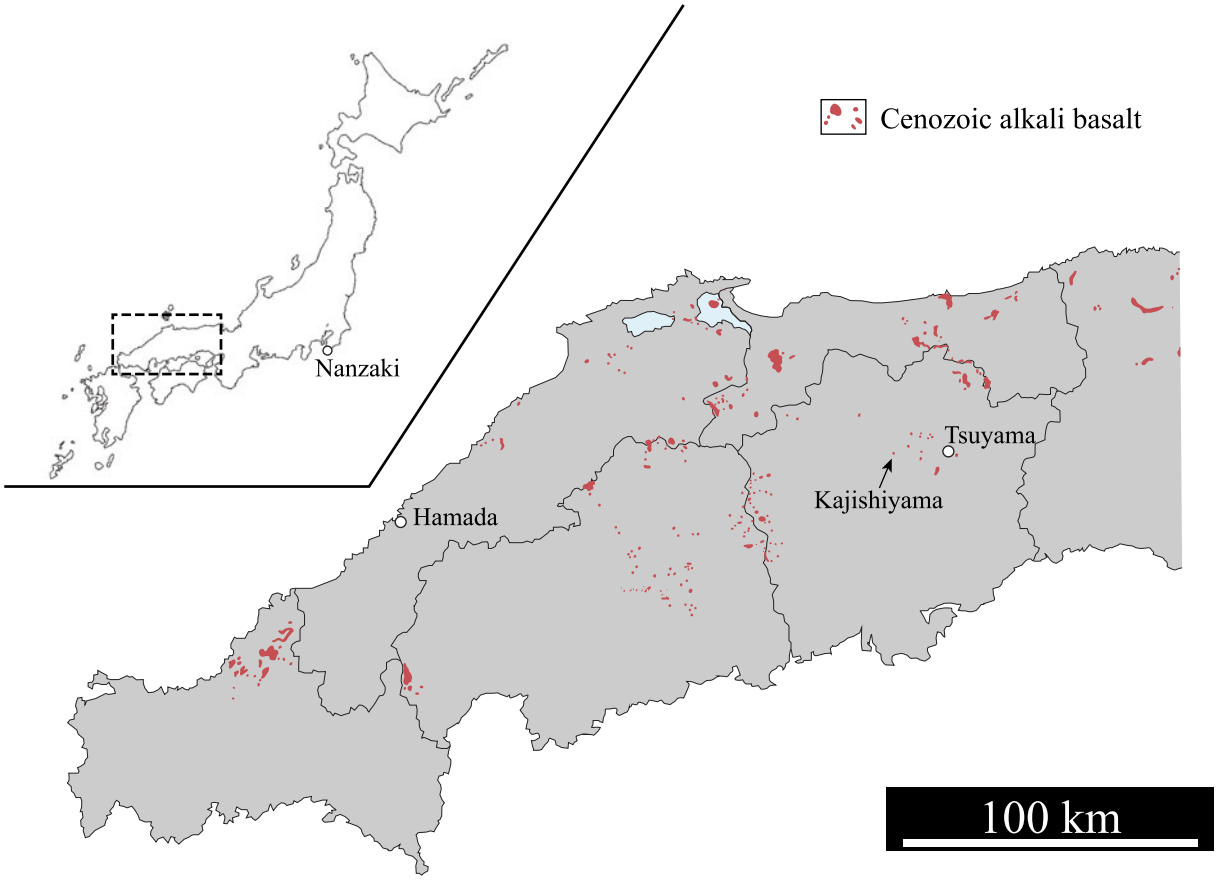

Figure 1. Distribution of Cenozoic alkali basalts in Chugoku region, southwest Japan (modified from Takamura, 1973) showing the location of Hamada and Kajishiyama. Note the nephelinite distributions at Hamada are too small to appear in the figure.

https://doi.org/10.1180/mgm.2023.32 Published online by Cambridge University Press

collected for detailed analysis are referred to as follows: fine grained (KJ-01, 02), medium grained (KJ-03, 04, 05, 06, 07) and coarse grained (KJ-08, 09). The grain size was determined by eye and thin-section observation. The mean grain size of the groundmass minerals in Kajishiyama fine-grained basanites is: 5 μm for spinel and 20–25 μm for plagioclase. In medium-grained basanites the mean is 7–8 μm for spinel and 40–60 μm for plagioclase and in the coarse-grained basanites the mean grain size of the groundmass is 10 μm for spinel and 60 μm for plagioclase (Fig. 2). The constituent minerals of these samples are essentially identical, irrespective of grain size.

The Kajishiyama basanite contains xenoliths and druses. The druses are classified into Type I and Type II. Type I is up to 20 mm in size and contains mainly euhedral zeolites such as phillipsite-K and 'hydroamesite', which have grown on the druse wall (Fig. 3a). Type II druse is <2 mm in size and normally filled with anhedral zeolites such as mesolite-K. Subhedral calcite or anhedral quartz occasionally coexist with mesolite-K in Type II druse. The maximum size of xenoliths is 20 mm for peridotites and 15 mm for the basement Sangun schists.

Olivine occurs as microphenocrysts (100–400 μm) and phenocrysts (up to 2.5 mm) in the Kajishiyama basanite; these are euhedral or subhedral and partly altered to iddingsite along cracks and the rim. The modal amount of olivine microphenocrysts and pheno crysts is ~10 vol.%. Augite occurs as microphenocrysts,

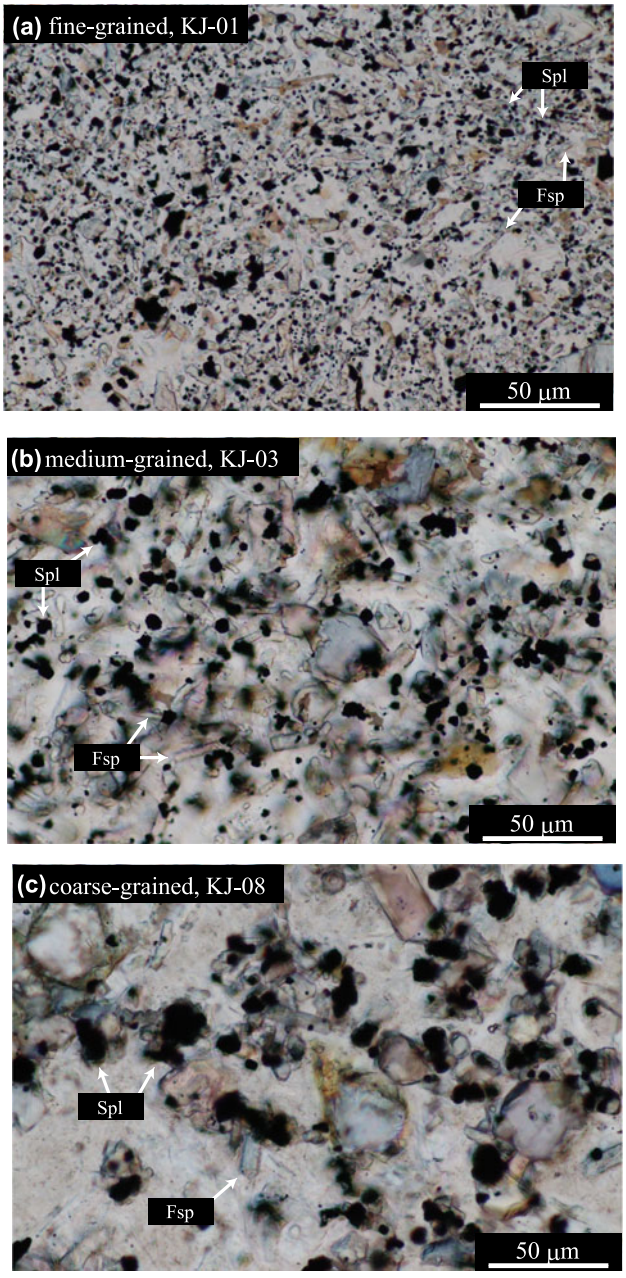

Figure 2. Grain size comparison of groundmass of Kajishiyama basanites. (a) Fine grained, KJ-01; (b) medium grained, KJ-03; and (c) coarse grained, KJ-08. Spl: spinel, Fsp: feldspar.

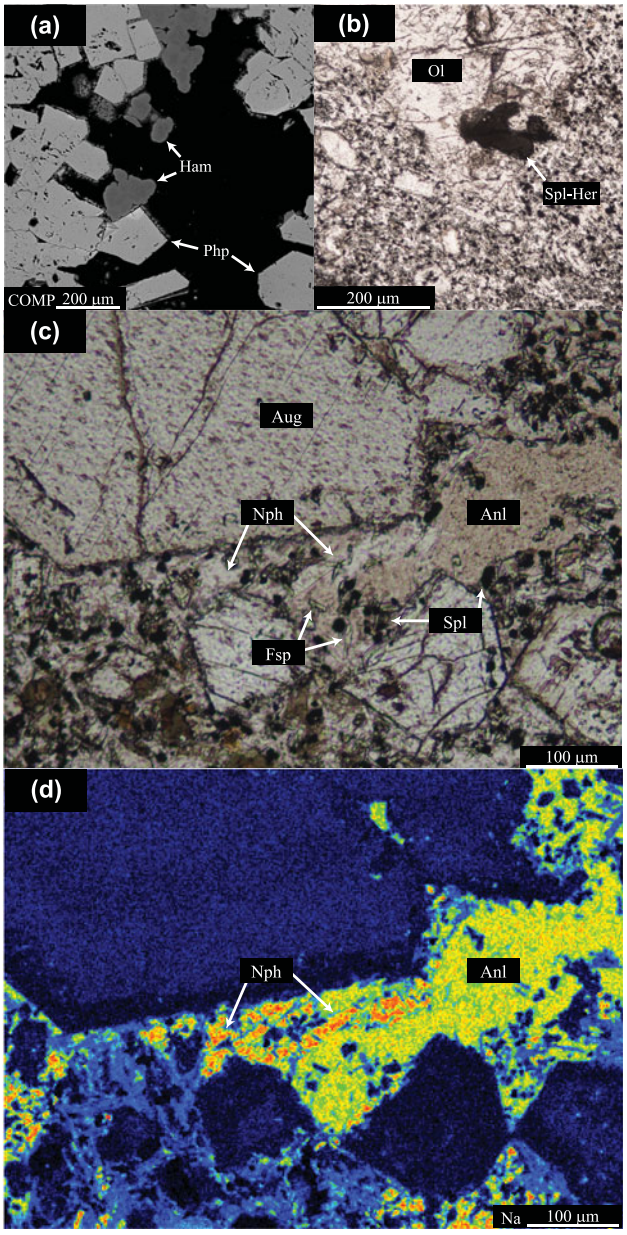

Figure 3. (a) Back-scattered electron (BSE) image of Type I druse (KJ-03). (b) Photomicrograph of spinel–hercynite solid solution and olivine as xenocrysts (KJ-08). The resorbed rim indicates the presence of xenocrysts. (c) Photomicrograph of nepheline and coexisting minerals (KJ-08). (d) Element-distribution map for Na in (c); the red zones are nephelines (KJ-08). Ham: hydroamesite, Php: phillipsite, Ol: olivine, Spl-Her: spinel–hercynite solid solution, Nph: nepheline, Aug: augite, Spl: spinel, Fsp: feldspar, Anl: analcime.

https://doi.org/10.1180/mgm.2023.32 Published online by Cambridge University Press

Table 1. Whole-rock compositions of Kajishiyama basanites.

Sample	KJ-01	KJ-02	KJ-03	KJ-04	KJ-05	KJ-06	KJ-07	KJ-08	KJ-09
Grain size	Fine	Fine	Medium	Medium	Medium	Medium	Medium	Coarse	Coarse
Major elements (wt.%)									
SiO_2	44.55	46.16	43.97	45.11	45.15	45.28	45.31	43.75	45.36
TiO_2	1.87	2.01	1.96	1.99	2.03	2.02	2.03	1.95	2.01
Al_2O_3	13.48	14.17	13.80	14.16	14.36	14.51	14.38	13.63	14.17
Fe_2O_3 *	12.89	11.41	12.53	12.24	11.99	11.64	11.87	13.09	11.75
MnO	0.18	0.19	0.19	0.19	0.19	0.19	0.19	0.19	0.19
MgO	10.17	10.65	9.87	10.67	10.29	10.25	10.27	9.94	10.85
CaO	10.35	10.57	11.03	10.94	11.29	11.51	11.12	11.18	11.08
Na_2O	3.46	3.92	3.45	3.45	3.30	3.01	3.36	2.89	2.62
K_2O	1.23	1.25	1.57	1.52	1.58	1.58	1.70	1.82	2.05
P_2O_5	0.53	0.59	0.58	0.59	0.61	0.61	0.61	0.58	0.60
Total	98.72	100.90	98.94	100.85	100.79	100.59	100.82	99.01	100.68
LOI	0.67	3.47	1.68	1.99	2.03	3.58	2.44	2.55	3.92
H_2O^-	0.44	0.91	0.48	0.58	0.60	0.89	0.58	0.79	0.78
Trace and rare earth elements (ppm)									
Sc	28	30	31	33	32	30	29	31	29
V	217	232	241	244	247	246	244	239	233
Cr	127	203	247	427	348	372	303	164	353
Co	46	50	53	49	50	48	50	47	51
Ni	149	210	167	204	190	173	192	130	220
Rb	31	60	53	56	56	78	61	63	76
Sr	1042	1076	1022	953	1115	1159	1042	989	1178
Y	24.9	29.3	26.3	27.4	30.1	26.1	26.2	26.7	27.4
Zr	184	203	187	190	211	188	191	193	201
Nb	65.3	71.9	69.6	67.0	75.8	71.7	70.5	73.0	74.6
Cs	0.6	1.0	0.8	1.4	1.4	1.3	1.1	0.5	1.0
Ba	1121	1285	1141	1123	1268	1207	1176	1195	1260
La	51.4	59.7	55.0	53.9	61.5	55.4	55.3	57.2	58.6
Ce	100.2	109.8	104.2	102.3	112.2	107.1	107.7	108.3	110.1
Pr	11.07	12.51	11.57	11.54	12.86	11.79	11.76	12.10	12.26
Nd	42.4	48.7	44.2	44.7	50.2	45.0	45.1	46.5	46.7
Sm	7.7	8.8	8.0	8.1	9.1	8.1	8.0	8.4	8.2
Eu	2.36	2.70	2.48	2.54	2.78	2.51	2.48	2.57	2.60
Gd	6.38	7.81	6.58	7.34	7.98	6.99	6.93	6.82	7.24
Tb	0.86	0.98	0.88	0.94	1.03	0.92	0.91	0.92	0.95
Dy	5.0	5.7	5.2	5.4	5.9	5.1	5.1	5.3	5.3
Ho	0.92	1.06	0.95	0.98	1.09	0.94	0.95	0.99	0.95
Er	2.6	2.9	2.7	2.7	3.0	2.6	2.6	2.7	2.7
Tm	0.355	0.376	0.355	0.354	0.392	0.351	0.332	0.359	0.352
Yb	2.16	2.41	2.30	2.24	2.48	2.25	2.22	2.29	2.28
Lu	0.303	0.337	0.331	0.329	0.372	0.326	0.322	0.331	0.316
Hf	4.2	4.5	4.1	4.3	4.8	4.3	4.3	4.4	4.3
Ta	3.34	3.91	3.55	3.60	4.18	3.61	3.62	3.78	3.91
Th	8.33	9.05	8.21	8.51	9.58	8.49	8.50	8.63	9.23

*Total iron as Fe_2O_3

~100–500 μm in size, showing short prismatic euhedral or subhedral habits in thin section, and also occurs as phenocrysts, up to 2.4 mm in size. Augite microphenocrysts and phenocrysts account for ~6 vol.%. Some augite microphenocrysts show zoning and partings. Additionally, subhedral or anhedral inclusions of spinel–hercynite solid solution (100–250 μm in size) and chromian spinels (30–65 μm in size) occur in the olivine and augite (Fig. 3b). We determined these spinel-group phenocrysts and microphenocrysts to be xenocrysts because their rims display evidence of resorption (Fig. 3b).

The groundmass is composed of Ca-bearing nepheline, olivine, augite, ulvöspinel, feldspars, zeolites and apatite (Fig. 3c). The Ca-bearing nepheline, anhedral and ~20 μm in size, fills interstices between phenocrysts and microphenocrysts and typically coexists with anhedral zeolites (Fig. 3c,d). Olivine and augite are subhedral-to-anhedral and 10–100 μm in size in the groundmass. Anhedral ulvöspinel in the groundmass is <10 μm in size and is sometimes included by microphenocrysts of olivine and augite, and groundmass minerals such as olivine, augite and feldspars. Both plagioclase and alkali feldspar occur as long prismatic crystals, 50 to 100 μm in length, in the groundmass, however plagioclase is more abundant than alkali feldspar. Zeolites are anhedral and interstitial to phenocrysts in the same manner as nepheline (Fig. 3c,d). Apatite appears as euhedral acicular crystals <10 μm in length.

According to the occurrence of constituent minerals, it is considered that the magmatic crystallisation sequence of the Kajishiyama basanite is: olivine + clinopyroxene + ulvöspinel → feldspars + apatite ± (olivine + augite + ulvöspinel) → nepheline.

Experimental methods

Whole-rock chemical analysis

Hand specimens with different grain sizes (KJ-01 to 09) were prepared for determining whole-rock compositions of the Kajishiyama basanite. Druses and xenoliths were removed to minimise

https://doi.org/10.1180/mgm.2023.32 Published online by Cambridge University Press

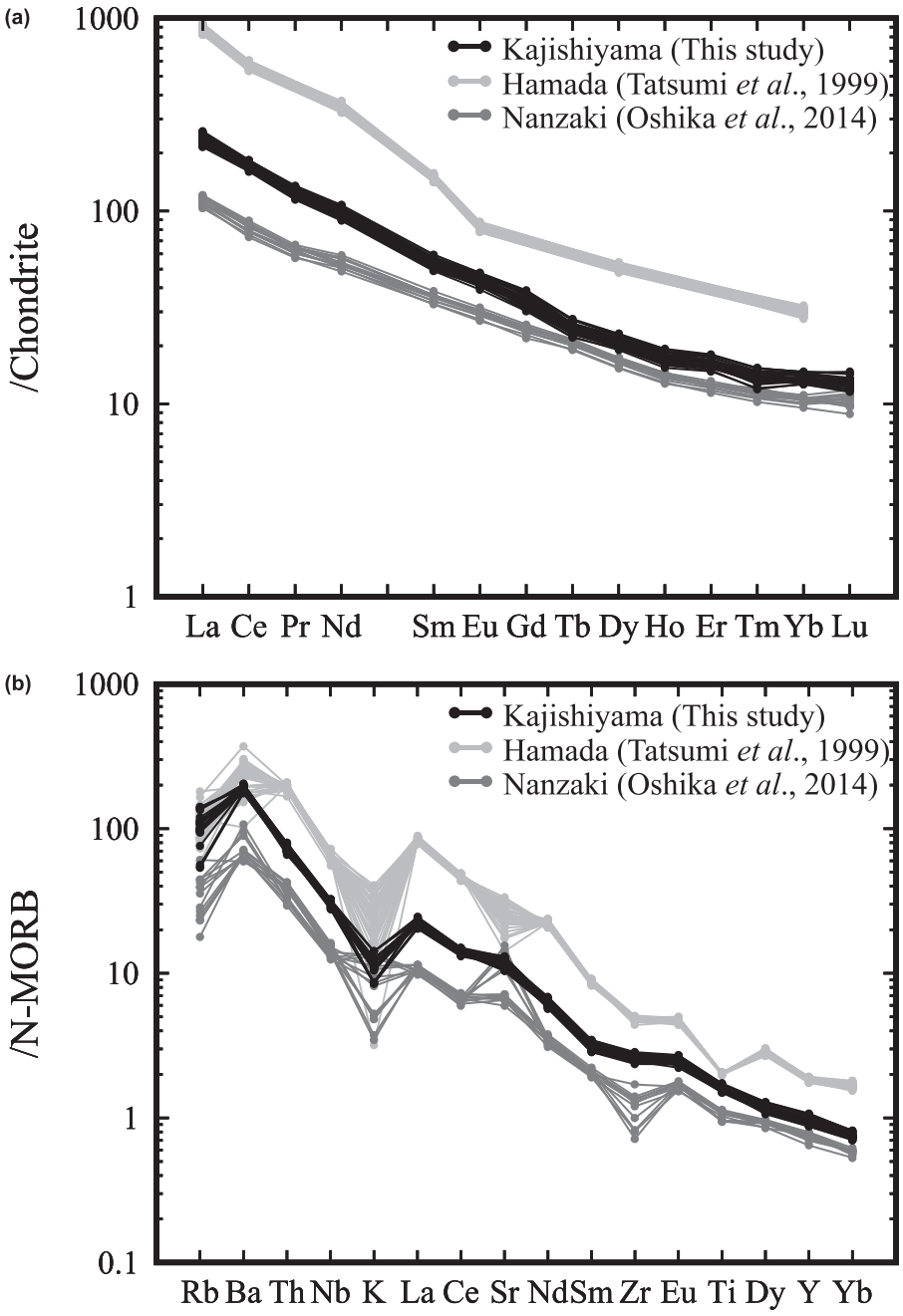

Figure 4. Trace element variation patterns of Kajishiyama basanites in comparison with related rocks in Japan. (a) Chondrite-normalised REE distribution patterns. (b) N-MORB-normalised trace-element patterns. Chondrite and N-MORB element abundances are from Sun and McDonough (1989). The data of Hamada nephelinites and Nanzaki basanites are from Tatsumi *et al.* (1999) and Oshika *et al.* (2014), respectively.

contamination, then the specimens were crushed and ground to powders using an iron mortar and an automatic agate mortar and pestle. The powdered samples were heated for 4 h at 900°C in an oven to determine the loss on ignition (LOI). Fused glass beads for major-element analysis were prepared with an alkali flux of $Li_2B_4O_7$. The flux-to-sample ratio was 10:1. The major-element contents were determined using a Rigaku ZSX Primus II X-ray fluorescence analyser at Kanazawa University, Japan. A Rh X-ray tube was used; tube voltage, specimen current and beam diameter were 50 kV, 50 mA and 30 mm, respectively.

The samples were analysed for trace and rare earth elements (REE) using an Agilent 7500s laser-ablation, inductively coupled plasma mass spectrometer (LA–ICP–MS) at Kanazawa University. The laser was UP-213 and was set to 5 Hz repetition, 100 μm spot size and 7–8 J/cm^2 energy density at target.

Composition analysis of minerals

Compositions of minerals in the Kajishiyama basanite were determined using the JEOL JXA-8800R electron probe micro-analyser at Kanazawa University. Nepheline and zeolite were analysed using an accelerating voltage, specimen current and beam diameter of 15 kV, 2 nA and 5 μm, respectively, to reduce damage by the electron beam. Other minerals were analysed using an accelerating voltage, specimen current and beam diameter of 20 kV, 20 nA and 2 μm, respectively. The standards (and elements) used were quartz (Si), $KTiPO_5$ (K, Ti and P), eskolaite (Cr), corundum (Al), fayalite (Fe), manganosite (Mn), wollastonite (Ca), periclase (Mg), jadeite (Na), NiO (Ni), baryte (Ba) and celestite (Sr). The ZAF method was used for data correction.

https://doi.org/10.1180/mgm.2023.32 Published online by Cambridge University Press

Table 2. Compositional data (wt.%) for Kajishiyama nepheline for medium (KJ-03) and coarse (KJ-08) grained samples. KJ-01 (fine grained) was measured but did not give reliable compositions because of the fine-grained character of the groundmass.

KJ-03 (medium)																	Range#	Mean
Wt.%	1	2	3	4	5	6	7	8	9	10	11	12	13	14	15	Range	*n* = 33	
SiO_2	46.29	45.23	47.52	45.28	45.48	46.05	45.11	46.16	46.17	45.09	45.44	45.17	46.57	46.96	46.61	45.09–47.52	45.09–48.00	45.15
TiO_2	0.03	0.05	0.04	n.d.	0.07	0.15	0.11	0.06	n.d.	0.19	0.04	0.06	0.13	n.d.	n.d.	0.00–0.19	0.00–0.19	0.06
Al_2O_3	31.48	32.15	31.19	31.71	32.12	31.03	32.62	32.21	31.38	31.96	31.56	32.24	31.38	31.53	31.72	31.03–32.62	30.59–32.62	30.52
Cr_2O_3	n.d.	n.d.	n.d.	n.d.	0.10	0.11	0.12	n.d.	n.d.	n.d.	n.d.	0.18	n.d.	0.17	0.12	0.00–0.18	0.00–0.18	0.04
Fe_2O_3 *	0.60	0.55	0.47	0.71	0.67	0.79	0.88	0.55	0.58	0.68	0.42	0.51	0.42	0.68	0.72	0.42–0.88	0.36–0.88	0.61
MnO	n.d.	0.01	0.02	0.02	0.12	n.d.	0.17	n.d.	n.d.	0.04	0.13	0.13	0.04	0.15	0.28	0.00–0.28	0.00–0.28	0.05
MgO	0.03	n.d.	0.01	0.04	n.d.	0.28	0.03	n.d.	0.07	0.16	0.01	n.d.	0.06	0.15	0.17	0.00–0.28	0.00–0.41	0.13
CaO	1.52	1.28	0.95	1.84	1.48	1.79	1.06	1.20	1.64	1.62	1.59	1.00	0.99	1.34	1.61	0.95–1.84	0.93–2.31	1.43
SrO	n.d.	n.d.	n.d.	0.08	n.d.	0.15	n.d.	n.d.	0.59	0.29	n.d.	0.59	0.29	n.d.	0.15	0.00–0.59	0.00–0.81	0.15
BaO	0.01	0.01	0.04	0.11	0.11	n.d.	n.d.	n.d.	n.d.	n.d.	0.19	n.d.	n.d.	n.d.	n.d.	0.00–0.19	0.00–0.23	0.05
Na_2O	15.11	15.82	15.79	15.58	16.12	14.82	15.80	15.55	14.82	15.09	15.56	16.12	15.74	14.79	14.83	14.79–16.12	14.01–16.75	15.04
K_2O	4.33	4.37	3.77	4.36	4.17	4.18	4.48	3.86	4.68	4.67	4.46	3.87	4.10	4.18	4.07	3.77–4.68	2.96–4.68	3.67
Total	99.40	99.48	99.79	99.74	100.43	99.35	100.39	99.58	99.93	99.78	99.38	99.86	99.71	99.94	100.28			99.92
Apfu based on O = 32																		
Si^{4+}	8.815	8.641	8.970	8.653	8.625	8.789	8.556	8.752	8.792	8.613	8.705	8.613	8.844	8.870	8.798	8.556–8.970	8.556–9.057	8.820
Ti^{4+}	0.005	0.008	0.005	-	0.010	0.022	0.016	0.009	-	0.028	0.005	0.008	0.018	-	-	0.000–0.028	0.000–0.028	0.009
Al^{3+}	7.066	7.238	6.938	7.142	7.180	6.980	7.293	7.197	7.044	7.196	7.126	7.246	7.025	7.020	7.057	6.938–7.293	6.816–7.293	7.023
Cr^{3+}	-	-	-	-	0.014	0.017	0.019	-	-	-	-	0.026	-	0.025	0.019	0.000–0.026	0.000–0.026	0.006
Fe^{3+}	0.086	0.079	0.066	0.103	0.096	0.114	0.126	0.078	0.084	0.098	0.060	0.073	0.059	0.097	0.102	0.059–0.126	0.051–0.126	0.088
Mn^{2+}	-	0.002	0.004	0.003	0.019	-	0.027	-	-	0.006	0.021	0.021	0.006	0.024	0.045	0.000–0.045	0.000–0.045	0.008
Mg^{2+}	0.008	0.000	0.003	0.011	-	0.080	0.009	-	0.019	0.044	0.003	-	0.016	0.041	0.047	0.000–0.080	0.000–0.117	0.037
Ca^{2+}	0.309	0.261	0.193	0.376	0.300	0.366	0.215	0.243	0.334	0.331	0.325	0.203	0.202	0.271	0.325	0.193–0.376	0.188–0.467	0.304
Sr^{2+}	-	-	-	0.009	-	0.016	-	-	0.065	0.033	-	0.065	0.032	-	0.016	0.000–0.065	0.000–0.087	0.016
Ba^{2+}	0.001	0.001	0.003	0.009	0.008	-	-	-	-	-	0.014	-	-	-	-	0.000–0.014	0.000–0.017	0.004
Na^{+}	5.578	5.860	5.778	5.774	5.928	5.486	5.811	5.715	5.474	5.589	5.782	5.959	5.796	5.417	5.428	5.417–5.959	5.136–6.116	5.679
K^{+}	1.053	1.065	0.908	1.063	1.009	1.017	1.085	0.932	1.138	1.139	1.090	0.941	0.992	1.008	0.981	0.908–1.139	0.711–1.139	0.916
Ne**	69.09	72.24	71.75	69.51	72.32	68.59	74.13	72.57	66.64	69.41	69.86	74.09	71.45	70.05	69.93	66.64–74.13	64.77–75.17	70.71
Ks	13.04	13.13	11.27	12.80	12.31	12.72	13.84	11.84	13.85	14.14	13.17	11.70	12.23	13.03	12.64	11.27–14.14	8.69–14.14	11.40
CaNe	7.68	6.46	4.85	9.48	7.52	9.56	5.50	6.16	9.72	9.03	8.20	6.68	5.77	7.00	8.78	4.85–9.72	4.85–12.53	8.08
Qz	10.19	8.16	12.12	8.21	7.85	9.13	6.54	9.43	9.79	7.42	8.76	7.53	10.55	9.91	8.66	6.54–12.12	6.54–12.53	9.82
$\Delta Al^{cc}/\Delta T^{ch}$	1.127	1.130	1.124	1.129	1.130	1.087	1.132	1.128	1.127	1.132	1.128	1.131	1.126	1.127	1.129			1.125

https://doi.org/10.1180/mgm.2023.32 Published online by Cambridge University Press

KJ-08 (coarse)

Wt.%	1	2	3	4	5	6	7	8	9	10	11	12	13	14	15	16	17	Max Ca	Range
SiO_2	47.24	46.20	46.66	46.70	48.00	46.08	47.05	46.14	47.67	47.52	47.71	47.29	46.92	47.28	47.69	47.95	46.84	47.18	46.08–48.00
TiO_2	0.16	n.d.	0.07	0.13	0.06	0.05	0.04	0.09	0.08	0.06	n.d.	n.d.	0.02	0.16	0.04	0.04	n.d.	n.d.	0.00–0.16
Al_2O_3	30.94	31.31	31.59	31.72	30.83	31.86	31.38	31.45	30.65	31.26	31.65	31.36	31.46	30.86	30.59	31.13	30.86	31.35	30.59–31.86
Cr_2O_3	n.d.	n.d.	n.d.	0.05	n.d.	n.d.	n.d.	n.d.	n.d.	0.09	0.04	0.15	n.d.	n.d.	0.03	0.02	0.05	0.02	0.00–0.15
Fe_2O_3 *	0.61	0.71	0.81	0.75	0.36	0.65	0.77	0.61	0.67	0.57	0.47	0.53	0.49	0.87	0.51	0.81	0.55	0.47	0.36–0.87
MnO	n.d.	0.10	n.d.	n.d.	0.04	0.02	0.16	0.08	n.d.	n.d.	n.d.	n.d.	n.d.	n.d.	n.d.	n.d.	n.d.	n.d.	0.00–0.16
MgO	0.25	0.19	0.19	0.16	0.20	0.23	0.30	0.03	0.13	0.07	0.05	0.10	0.14	0.41	0.35	0.26	0.30	0.06	0.03–0.41
CaO	1.16	2.18	1.13	1.16	1.81	1.34	1.21	1.68	1.99	1.35	1.06	0.93	1.90	1.89	2.27	1.64	1.67	2.31	0.93–2.31
SrO	n.d.	0.33	0.25	n.d.	n.d.	n.d.	n.d.	n.d.	0.65	n.d.	0.81	0.15	0.37	n.d.	0.22	n.d.	n.d.	n.d.	0.00–0.81
BaO	0.09	0.02	n.d.	n.d.	0.08	0.08	0.01	0.06	0.05	0.09	0.03	n.d.	0.23	0.03	0.18	0.10	0.13	0.17	0.00–0.23
Na_2O	16.75	14.88	16.23	16.37	14.58	16.58	16.05	16.48	14.64	16.17	15.92	16.12	15.54	14.18	14.01	15.06	15.07	14.43	14.01–16.75
K_2O	2.96	3.77	3.80	3.12	3.37	3.28	3.36	3.49	3.58	3.32	3.24	3.03	3.17	3.39	3.66	3.61	3.58	3.82	2.96–3.82
Total	100.15	99.68	100.72	100.16	99.33	100.15	100.33	100.09	100.10	100.49	100.98	99.65	100.25	99.07	99.55	100.62	99.04	99.81	
Apfu based on O = 32																			
Si^{4+}	8.899	8.786	8.784	8.794	9.057	8.711	8.852	8.746	8.995	8.918	8.921	8.924	8.849	8.958	9.020	8.973	8.917	8.912	8.711–9.057
Ti^{4+}	0.023	-	0.009	0.019	0.009	0.007	0.006	0.012	0.011	0.008	-	-	0.003	0.023	0.006	0.006	-	-	0.000–0.023
Al^{3+}	6.869	7.016	7.010	7.041	6.857	7.099	6.958	7.025	6.816	6.914	6.974	6.973	6.993	6.891	6.818	6.864	6.924	6.980	6.816–7.099
Cr^{3+}	-	-	-	0.007	-	-	-	-	-	0.013	0.006	0.022	-	-	0.005	0.002	0.007	0.003	0.000–0.022
Fe^{3+}	0.086	0.102	0.115	0.107	0.051	0.093	0.110	0.087	0.095	0.081	0.066	0.075	0.070	0.124	0.073	0.114	0.078	0.067	0.051–0.124
Mn^{2+}	-	0.016	-	-	0.006	0.003	0.025	0.013	-	-	-	-	-	-	-	-	-	-	0.000–0.025
Mg^{2+}	0.069	0.053	0.053	0.044	0.055	0.063	0.085	0.009	0.036	0.018	0.014	0.028	0.039	0.117	0.098	0.073	0.085	0.017	0.009–0.117
Ca^{2+}	0.233	0.444	0.228	0.234	0.366	0.271	0.243	0.340	0.402	0.272	0.213	0.188	0.384	0.383	0.459	0.329	0.341	0.467	0.188–0.467
Sr^{2+}	-	0.036	0.027	-	-	-	-	-	0.071	-	0.087	0.016	0.040	-	0.024	-	-	-	0.000–0.087
Ba^{2+}	0.007	0.001	-	-	0.006	0.006	0.001	0.004	0.003	0.006	0.002	-	0.017	0.002	0.013	0.008	0.010	0.013	0.000–0.017
Na^{+}	6.116	5.487	5.924	5.977	5.335	6.076	5.852	6.056	5.355	5.885	5.771	5.899	5.683	5.208	5.137	5.463	5.564	5.286	5.136–6.116
K^{+}	0.711	0.913	0.912	0.750	0.811	0.791	0.807	0.843	0.862	0.795	0.773	0.728	0.763	0.819	0.883	0.861	0.869	0.919	0.711–0.919
Ne**	74.71	67.79	73.13	75.11	67.73	75.17	74.29	72.28	65.59	72.05	71.56	74.47	69.61	68.47	64.77	69.27	69.90	65.50	64.77–75.17
Ks	8.69	11.28	11.26	9.42	10.29	9.78	10.25	10.06	10.56	9.74	9.58	9.19	9.34	10.77	11.13	10.92	10.92	11.39	8.69–11.39
CaNe	5.87	11.90	6.28	5.89	9.45	6.84	6.19	8.22	11.67	6.81	7.49	5.16	10.81	10.14	12.53	8.54	8.80	11.89	5.16–12.53
Qz	10.73	9.03	9.32	9.58	12.53	8.20	9.27	9.43	12.18	11.40	11.37	11.17	10.24	10.62	11.57	11.27	10.38	11.22	8.20–12.53
$\Delta Al^{cc}/\Delta T^{ch}$	1.126	1.129	1.128	1.126	1.123	1.130	1.128	1.127	1.123	1.124	1.125	1.125	1.126	1.126	1.123	1.124	1.125	1.125	

#This Range is all data - coarse and medium. *Total iron as Fe_2O_3; **Calculation of Ne–Ks–CaNe–Qz component and $\Delta Al^{cc}/\Delta T^{ch}$ follows Henderson and Oliveria (2022).
n.d. – not detected

Table 3. Reference list for samples plotted in Fig. 5 and Fig. 7.

Reference	Rock type	Locality	Ca-rich nepheline?*	Melilite?	Figure
This study	basanite	Kajishiyama, Southwestern Japan	yes	no	Fig. 5, 7
Hirai and Arai (1983)	basanite	Kajishiyama, Southwestern Japan	yes	no	Fig. 5, 7
	basanite	Noyamadake, Southwestern Japan	yes	no	Fig. 5, 7
Oshika *et al.* (2014)	basanite	Nanzaki, Japan	yes	no	Fig. 5, 7
Brown and Carmichael (1969)	basanite	Korath Range, Southern Ethiopia	yes	no	Fig. 5, 7
Wilkinson and Hensel (1994)	basanite	Gunnedah, north-eastern New South Wales	yes	no	Fig. 5, 7
Perepelov *et al.* (2007)	basanite	Western Kamchatka	yes	no	Fig. 5, 7
Garcia *et al.* (1986)	basanite	Honolulu volcanics, Oahu, Hawaii	-	-	Fig. 7
Gibson *et al.* (1999)	basanite	Banhadao, southern Brazil	-	-	Fig. 7
	basanite	Cerro Azul, Juquiá, southern Brazil	-	-	Fig. 7
Paslick *et al.* (1996)	basanite	Gelai, northern Tanzanian	-	-	Fig. 7
	basanite	Mosonik, northern Tanzanian	-	-	Fig. 7
	basanite	Ngorongoro, northern Tanzanian	-	-	Fig. 7
Tatsumi *et al.* (1999)	melilite–olivine nephelinite	Hamada, Southwestern Japan	no	yes	Fig. 5
Hamada (2011)	melilite–olivine nephelinite	Hamada, Southwestern Japan	no	yes	Fig. 5
Hamada *et al.* (2019)	melilite–olivine nephelinite	Hamada, Southwestern Japan	no	yes	Fig. 5
Sharygin *et al.* (2012)	combeite–bearing nephelinite	Oldoinyo Lengai, Tanzania	no	no	Fig. 5
Peterson (1989)	wollastonite–combeite nephelinite	Oldoinyo Lengai, Tanzania	no	no	Fig. 5
Comin-Chiaramonti *et al.* (1991)	nephelinite	Nemby, Eastern Paraguay	yes	no	Fig. 5
Wilkinson and Stolz (1983)	olivine melilite nephelinite	Moiliili, Oahu, Hawaii	no	yes	Fig. 5
Zaitsev *et al.* (2012)	nephelinite	Sadiman, Crater Highlands area, northern Tanzania	no	no	Fig. 5
Wittke and Holm (1996)	basanitic nephelinite	House Mountain volcano, North-central Arizona, USA	yes	no	Fig. 5
Dawson (1998)	wollastonite nephelinite	Oldoinyo Lengai, Tanzania	no	yes	Fig. 5
Blancher *et al.* (2010)	nephelinite	Messum complex, Etendeka province, Northwestern Namibia	no	-	Fig. 5
Antao and Hassan (2010)	nepheline syenite	Nephton, Bancroft area, southeastern Ontario	no	-	Fig. 5
	magmatic origin	Davis Hill, Bancroft area, southeastern Ontario	no	-	Fig. 5
Hassan *et al.* (2003)	nepheline–scapolite–albite–biotite gneiss	Egan Chute on the York River, near Bancroft, Ontario, Canada	yes	-	Fig. 5
Sahama (1952)	–	Southern slope of Mt. Ninagongo, Lake Kivu National Park Area, Belgian Congo	yes	-	Fig. 5
Vulić *et al.* (2011)	pegmatite	Lille Arøya island, Langesundsfjord, South Norway	no	-	Fig. 5
	pegmatite inside larvikite	Treschow-Fritzøe (Almenningen) quarry, Tvedalen, Langesundsfjord, South Norway	no	-	Fig. 5
	urtite	Tertiary Gardiner Complex in the East Greenland	no	-	Fig. 5
	alkaline pegmatite	Singertât complex, South-east Greenland	no	-	Fig. 5
	urtite	Singertât complex, South-east Greenland	no	-	Fig. 5
	ijolite	Singertât complex, South-east Greenland	no	-	Fig. 5
	cancrinite–ijolite	Iivaara alkaline complex in North Finland	no	-	Fig. 5
Balassone *et al.* (2014)	pumice	Somma-Vesuvius volcanic complex, Southern Italy	yes	no	Fig. 5
	magmatic ejectum	Somma-Vesuvius volcanic complex, Southern Italy	yes	no	Fig. 5
	metamorphic ejectum	Somma-Vesuvius volcanic complex, Southern Italy	yes	no	Fig. 5
Tait *et al.* (2003)	hydrothermal veinlet	Khibina–Lovozero complex, Kola peninsula, Russia	no	-	Fig. 5
	pegmatite in nepheline syenite	near Bancroft, Ontario, Canada	no	-	Fig. 5
	marble blocks in volcanic ejecta	Monte Somma, Mount Vesuvius, Italy	yes	-	Fig. 5
Antao and Nickolls (2018)	–	Mount Nyiragongo, Eastern Congo, Africa	no	no	Fig. 5
	–	Oldoinyo Lengai, Tanzania	yes	yes	Fig. 5
Henderson and Gibb (1983)	theralite	Papeno Valley, Tahiti	yes	no	Fig. 5
	crinanite	Howford Bridge sill, Ayrshire, Scotland	yes	no	Fig. 5
Blancher *et al.* (2010)	therelite	Messum complex, Etendeka province, Northwestern Namibia	yes	-	Fig. 5
	nepheline diorite	Messum complex, Etendeka province, Northwestern Namibia	yes	-	Fig. 5
	nepheline monzonite	Messum complex, Etendeka province, Northwestern Namibia	yes	-	Fig. 5
	nepheline syenite	Messum complex, Etendeka province, Northwestern Namibia	yes	-	Fig. 5
	peralkaline syenite	Messum complex, Etendeka province, Northwestern Namibia	no	-	Fig. 5
Wittke and Holm (1996)	nepheline monzosyenite	House Mountain volcano, North-central Arizona, America	yes	no	Fig. 5
	syenitic urtite	House Mountain volcano, North-central Arizona, America	yes	no	Fig. 5
	feldspar ijolite	House Mountain volcano, North-central Arizona, America	yes	no	Fig. 5

* The threshold for 'Ca-rich' was set at 0.5 wt.% CaO.

Whole-rock compositions

The whole-rock compositions of the Kajishiyama basanite samples are given in Table 1. The SiO_2 content is 43.75–46.16 wt.%. The Kajishiyama basanite is confirmed to be silica-undersaturated and is characterised by high total alkalis, Sr and Ba contents. The chondrite-normalised REE distribution patterns (Fig. 4a) are similar to those of the Nanzaki basanite (Oshika *et al.*, 2014) and the Hamada nephelinite (Tatsumi *et al.*, 1999) (Fig. 1), showing high concentrations of incompatible elements. The Kajishiyama basanites were possibly formed by a low degree of partial melting of a source asthenospheric mantle peridotite, considering the high contents of incompatible elements and the

https://doi.org/10.1180/mgm.2023.32 Published online by Cambridge University Press

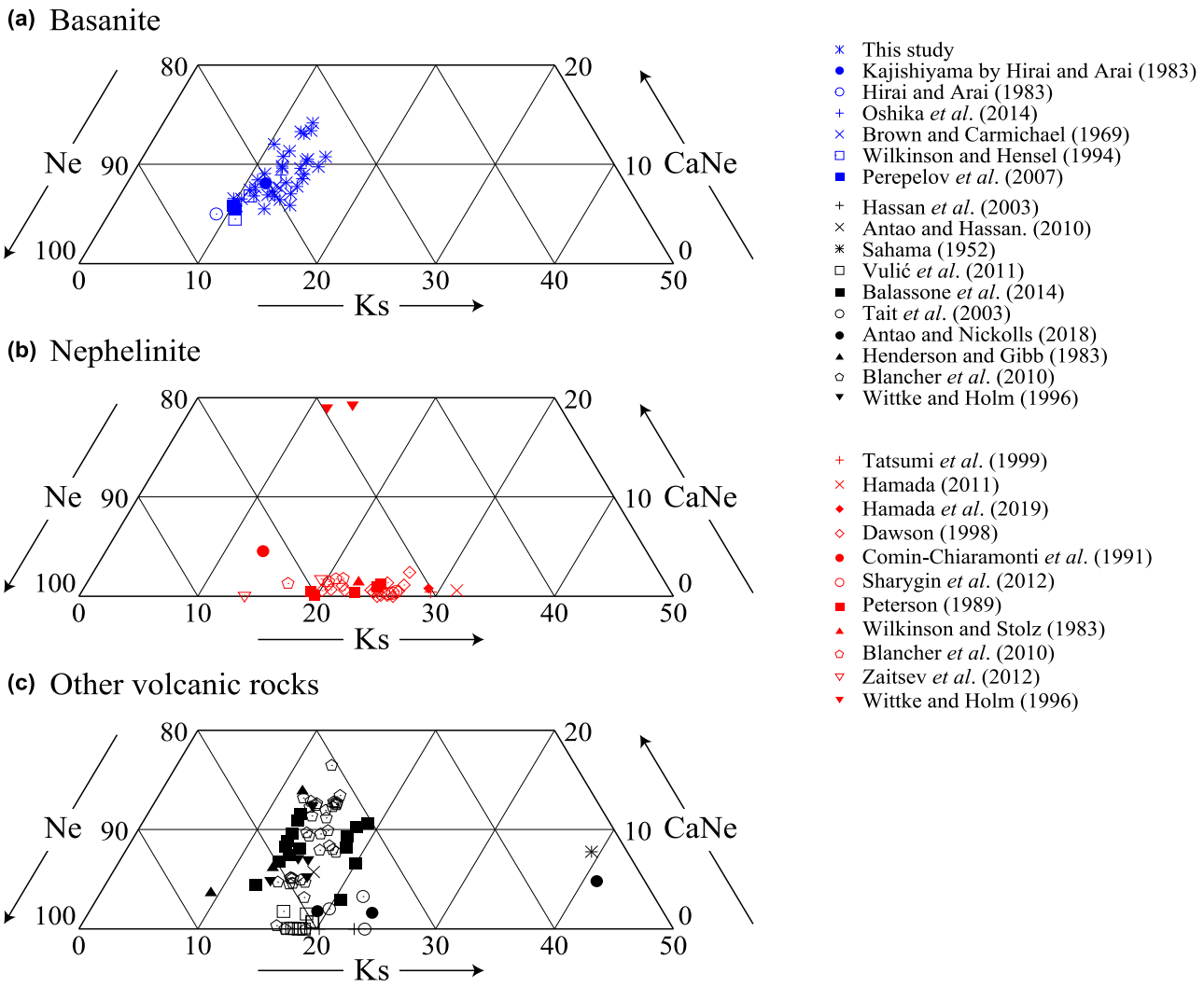

Figure 5. Compositions of nepheline in the Ca-Nepheline–Nepheline–Kalsilite ternary diagram: (a) nepheline compositions of basanites; (b) nepheline compositions of nephelinites; and (c) nepheline compositions of theralites, urtites, syenites and ijolites. The references for data plotted in this figure are listed in Table 3.

low FeO*/MgO ratio (*total iron as FeO) of the whole-rock composition and the high Fo contents of olivine (up to 90 mol.%; see 'Mineral compositions' below). There is no Eu anomaly, which suggests formation by removal solely of olivine and clinopyroxene, without plagioclase, at an early stage of fractional crystallisation of the basanite (see Discussion section). N-MORB-normalised trace-element patterns (Fig. 4b) also show a similarity between Kajishiyama basanite, Nanzaki basanite and Hamada nephelinite, with a depletion in alkalis such as Rb and K. This depletion is usually ascribed to the selective loss during deuteric hydrothermal alteration processes (Tatsumi *et al.*, 1999).

The Kajishiyama basanites of different grain size have similar whole-rock compositions though differing water content. The coarser grained sample has a higher LOI, e.g. 0.67 (KJ-01; fine), 1.68–3.58 (medium) and 2.55–3.92 wt.% (coarse) (Table 1). Note that KJ-02 has a high LOI (3.47 wt.%) even though it is fine-grained. This could be because druses were not removed completely prior to crushing. In these basanites, LOI is ascribed to the presence of altered olivine, zeolite in groundmass and druse and calcite in druse. However the degree of alteration between the basanite samples shows no difference, the amount of calcite in druse is negligible and the druses were removed during preparation. Therefore, we interpret the LOI to be mainly due to the presence of groundmass zeolites, consistent with the observations of Hirai and Arai (1986), which is that zeolites were formed by the reaction between the initial nepheline and deuteric fluid related to the deuteric alteration of the solidified basanite. The alkali depletion is at the same stage as the deuteric alteration of nepheline (Hirai and Arai, 1986).

Mineral compositions

Nepheline

Compositions of nepheline are listed in Table 2. The nepheline contains up to 2.31 wt.% CaO (0.467 atoms per formula unit: apfu). Overall, the Kajishiyama Ca-bearing nepheline contains 14.01–16.75 wt.% Na_2O (5.136–6.112 apfu) and 2.96–4.68 wt.% K_2O (0.711–1.139 apfu). Although the ideal Na to K ratio of nepheline is 3:1, it is ~5.5:1 in these nephelines. Moreover, the Ca-bearing nepheline contains up to 0.88 wt.% Fe_2O_3

https://doi.org/10.1180/mgm.2023.32 Published online by Cambridge University Press

Table 4. Representative compositions of associated minerals of the Kajishiyama basanite. Compositional data for olivine, augite, spinel-group minerals and plagioclase are from KJ-03, and compositional data for alkali feldspar and zeolite-group minerals are from KJ-08.

	Olivine		Augite		Spinel–hercynite**	Chromian spinel**		Ulvöspinel	Feldspar		Zeolite		
	core	rim	core	rim		core	rim		Plagioclase	Alkali feldspar	Analcime	Phillipsite-K	Stilbite-Na
Wt.%													
SiO_2	40.16	37.72	49.25	45.16	0.02	0.06	0.08	0.01	53.48	63.67	54.59	43.68	59.82
TiO_2	0.03	0.05	1.09	3.01	0.42	0.69	3.08	18.59	0.16	0.15	0.07	0.01	0.06
Al_2O_3	0.04	0.10	8.06	9.31	54.48	42.83	34.86	2.11	27.83	20.65	22.48	25.82	21.81
Cr_2O_3	n.d.	n.d.	0.01	n.d.	0.03	20.66	12.88	n.d.	n.d.	n.d.	0.10	n.d.	n.d.
Fe_2O_3*	-	-	1.74	2.91	12.28	6.04	14.39	27.90	-	-	-	-	-
FeO*	15.46	26.73	4.20	4.73	18.86	12.70	25.49	43.43	1.01	0.33	0.09	0.13	0.37
NiO	0.11	0.03	0.02	0.04	0.03	0.14	0.04	0.03	0.21	n.d.	0.10	n.d.	0.01
MnO	0.28	0.70	0.14	0.13	0.20	0.23	0.52	0.76	0.04	n.d.	0.10	n.d.	n.d.
MgO	44.52	34.05	14.31	11.48	14.41	17.25	9.11	1.41	0.18	0.09	0.12	0.06	n.d.
CaO	0.32	0.44	20.01	22.98	0.02	0.04	0.13	0.22	8.86	2.03	0.82	9.35	0.28
SrO	n.d.	n.d.	n.d.	n.d.	0.02	0.18	0.14	n.d.	0.63	n.d.	n.d.	0.16	n.d.
BaO	0.03	0.01	0.04	0.02	n.d.	0.02	n.d.	0.06	0.27	0.60	n.d.	0.25	n.d.
Na_2O	n.d.	0.04	0.97	0.41	0.02	0.02	0.04	0.06	6.81	5.31	12.14	0.42	6.03
K_2O	n.d.	0.01	0.01	0.02	n.d.	n.d.	0.02	0.03	0.81	7.39	0.31	6.81	0.21
P_2O_5	0.04	n.d.	0.09	0.02	0.05	0.02	n.d.	n.d.	n.d.	n.d.	0.20	0.05	0.13
Total	100.98	99.86	99.94	100.22	100.82	100.88	100.77	94.61	100.29	100.22	91.11	86.72	88.71
Apfu	O = 4	O = 4	O = 6	O = 6	O = 32	O = 32	O = 32	O = 32	O = 8	O = 8	O = 6	O = 32	O = 72
Si^{4+}	1.001	1.006	1.803	1.684	0.004	0.014	0.019	0.002	2.448	2.882	2.011	9.426	26.123
Ti^{4+}	-	0.001	0.030	0.084	0.067	0.114	0.554	4.361	0.006	0.005	0.002	0.001	0.020
Al^{3+}	0.001	0.003	0.347	0.409	13.840	11.137	9.842	0.775	1.501	1.102	0.976	6.568	11.225
Cr^{3+}	-	-	-	-	0.004	3.603	2.440	-	-	-	0.003	-	-
Fe^{3+}	-	-	0.048	0.082	1.992	1.004	2.595	6.547	-	-	-	-	-
Fe^{2+}	0.322	0.596	0.129	0.148	3.399	2.344	5.108	11.326	0.039	0.013	0.003	0.023	0.134
Ni^{2+}	0.002	0.001	-	0.001	0.006	0.025	0.007	0.008	0.008	-	0.003	-	0.002
Mn^{2+}	0.006	0.016	0.004	0.004	0.037	0.043	0.106	0.200	0.002	-	0.003	-	-
Mg^{2+}	1.654	1.354	0.781	0.638	4.628	5.672	3.253	0.654	0.012	0.006	0.007	0.019	-
Ca^{2+}	0.008	0.012	0.785	0.918	0.004	0.010	0.032	0.073	0.435	0.098	0.033	2.162	0.129
Sr^{2+}	-	-	-	-	0.003	0.023	0.019	-	0.017	-	-	0.020	-
Ba^{2+}	-	-	0.001	-	-	0.002	-	0.008	0.005	0.011	-	0.021	-
Na^{+}	-	0.002	0.069	0.029	0.007	0.007	0.018	0.033	0.605	0.466	0.868	0.174	5.106
K^{+}	-	-	0.001	0.001	-	0.001	0.006	0.014	0.047	0.427	0.014	1.874	0.114
P^{5+}	0.001	-	0.003	0.001	0.009	0.003	-	-	-	-	0.006	0.010	0.048

*Fe_2O_3 and FeO of augite and spinel-group minerals were with adjustment of total cations to 4 for O = 6 and 24 for O = 32, respectively.
**Spinel–hercynite solid-solution samples and chromian spinels are xenocrysts.
n.d. – not detected

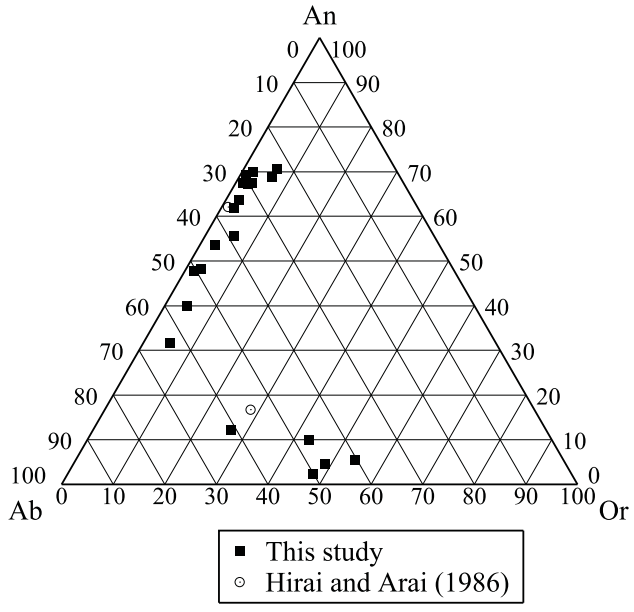

Figure 6. Compositions of feldspars in the Kajishiyama basanites from this study and Hirai and Arai (1986).

(as total Fe; 0.126 apfu). In addition, the excess silica component was detected in the Ca-bearing nepheline, as noted previously by Hirai and Arai (1983). The Ca and K contents of nepheline are slightly different between the medium-grained basanite (KJ-03) and coarse-grained basanite (KJ-08), i.e. nepheline from the former has lower Ca and higher K contents than the latter.

The end-member proportions of Ne (nepheline; $Na_8Al_8Si_8O_{32}$), Ks (kalsilite; $K_8Al_8Si_8O_{32}$) and CaNe (Ca nepheline; $\square_4^{Ca}Ca_4Al_8Si_8O_{32}$) components of the Ca-bearing nephelines from Kajishiyama together with nephelines from some other localities (Table 3) are plotted by rock type in Fig. 5. Figures 5a and 5b show nephelines are considerably enriched in Ca from basanites, including the Kajishiyama sample, compared to those from nephelinites, except for those from basanitic nephelinites (Wittle and Holm, 1996). Additionally, nephelines in theralite (Henderson and Gibb, 1983; Blancher *et al.*, 2010) might be rich in Ca, but nephelines in urtite (Vulić *et al.*, 2011; Wittle and Holm, 1996), syenite (Blancher *et al.*, 2010; Wittle and Holm, 1996) and ijolite (Vulić *et al.*, 2011; Wittle and Holm, 1996) have both Ca-rich and Ca-poor nephelines (Fig. 5c). More data are needed to confirm the trend of Ca in nepheline from these rocks.

https://doi.org/10.1180/mgm.2023.32 Published online by Cambridge University Press

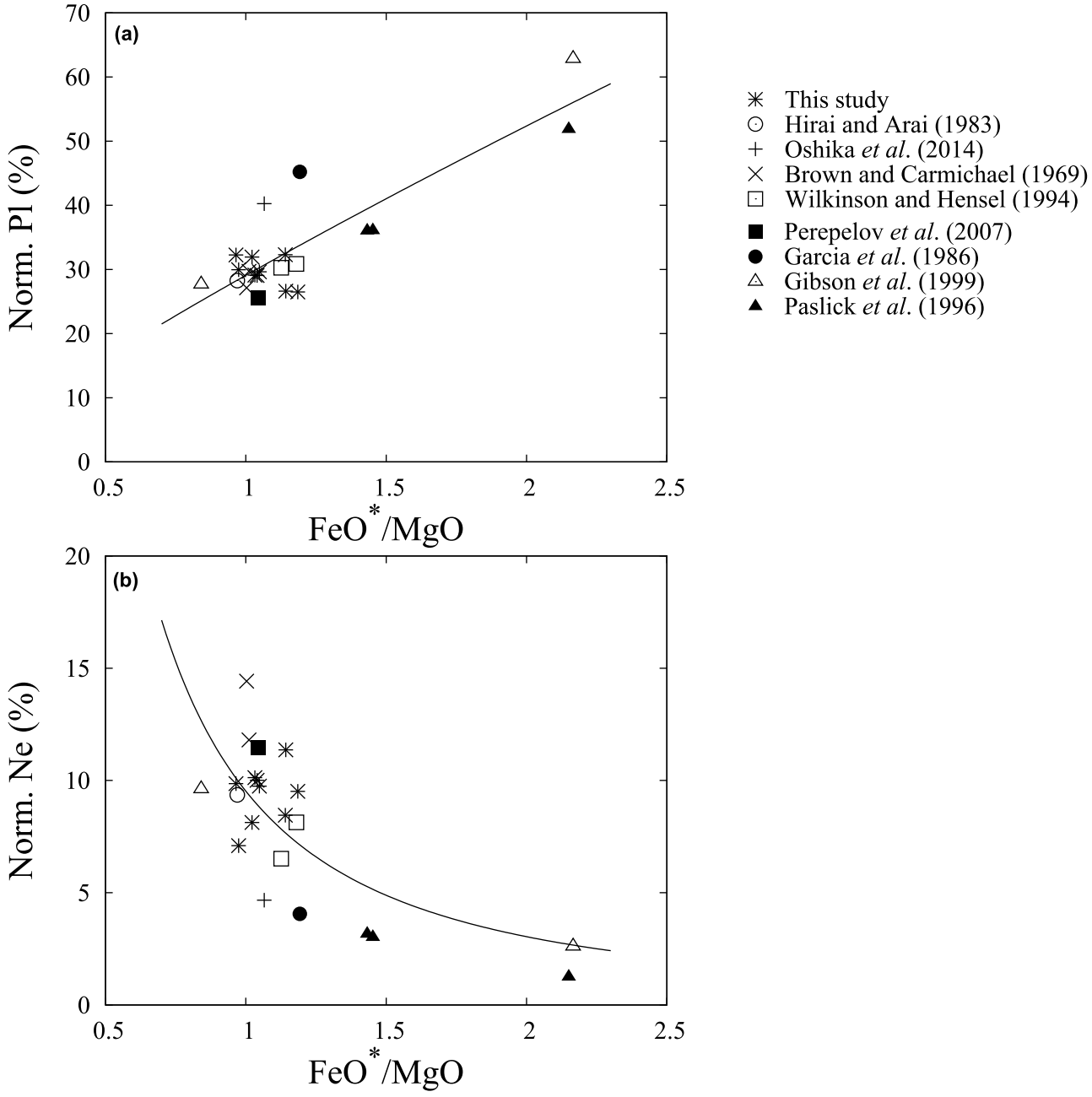

Figure 7. Fractionation trends of basanites. (a) Relationship between normative plagioclase and FeO*/MgO and (b) relationship between normative nepheline and FeO*/MgO. FeO*, total iron as FeO. Note – the MO93-3 sample was reported as 'basanite' by Paslick *et al.* (1996), however it is nephelinite according to the classification of Le Bas (1989) using $SiO_2 + Al_2O_3$ versus $CaO + Na_2O + K_2O$, so MO93-3 data is not shown here. The references for the data plotted in this figure are listed in Table 3.

Other minerals

Compositions of associated minerals are given in Table 4. Olivine phenocrysts show normal zoning with forsterite components of the core ($Fo_{82–90}$) higher than for the rim ($Fo_{65–77}$). Furthermore, the rim is enriched in MnO and CaO compared with the core, but NiO is lower. Additionally, Ti-rich augite phenocrysts, with or without zonal textures, were found in the Kajishiyama basanite. The rim of the zoned Ti-rich augite is enriched in TiO_2, Al_2O_3 and Fe compared with the core. Ulvöspinel, which occurs in the groundmass, contains 18.59 wt.% TiO_2. Plagioclase contains 31–71 mol.% anorthite component, and alkaline feldspars contain 27–54 mol.% orthoclase component (Fig. 6). SrO and BaO contents are up to 0.64 wt.% and 0.96 wt.% in the plagioclase and up to 0.34 wt.% and 1.23 wt.% in the alkali feldspar, respectively. Fine acicular apatite is too small to be analysed by microprobe. Analcime, phillipsite-K and stilbite-Na in the groundmass are characterised by high alkali contents.

Discussion

Chemical formula of the Kajishiyama Ca-bearing nepheline

The chemical formula of nepheline, especially the distribution of M^{3+} and M^{2+} cations in the nepheline structure, has been discussed in many publications. Hahn and Buerger (1955) and

https://doi.org/10.1180/mgm.2023.32 Published online by Cambridge University Press

Dollase (1970) investigated the crystal structure of natural nephelines, albeit without any reference to the Ca distribution. Donnay *et al.* (1959) suggested that Fe^{3+} substitutes for Si and Al in tetrahedral coordination to form an iron-nepheline component. They also suggested that the small amounts of Mg, Mn and Ti that might be present within the nepheline structure could substitute for Na, K and Ca. In addition, the occupancy of Mg, Fe^{2+}, Mn or Ti in the framework of nepheline and synthesised leucite was reported by Buerger (1954), Dollase and Thomas (1978) and Roedder (1951, 1952, 1978). Strontium and Ba occupy cavity sites (*A* and *B* channel) in a similar manner to analogue kalsilite structures with a stuffed-tridymite framework (Henderson and Taylor, 1982). Henderson (2020) concluded that smaller divalent cations (e.g. Mg and Mn) and Ti probably replace Si in the tetrahedral site, whereas larger cations such as Ca, Sr, Ba and Rb replace K and Na in cavity sites, and provided the protocol for nepheline formula calculation. Recently, Henderson and Oliveira (2022) modified this protocol in order to deal correctly with Fe^{2+}, Mg^{2+} and Mn^{2+} in tetrahedral sites; even small contents of these components in natural nephelines requires the corrected Henderson and Oliveira (2022) protocol to be applied.

Henderson (2020) and Henderson and Oliveira (2022) defined end-members of nepheline as Ne, Ks, CaNe and Q^{xs} (excess quartz; $\square_8^{Si}Si_{16}O_{32}$), and established a calculation protocol of end-member proportions and of vacancy proportions in the nepheline structure. There are two types of occupation of vacant sites (*A* and *B* channels), i.e. $\square^{Si}$ (caused by excess Si which takes into account the replacement of Al^{3+} by Fe^{2+}, Mg^{2+} and Mn^{2+} in tetrahedral sites) and $\square^{Ca}$ (caused by replacement of Na^+ and K^+ by Ca^{2+}, Sr^{2+} and Ba^{2+}). In this study, the highest-Ca nepheline has 8.912 apfu and 0.480 apfu of Si and Ca+Sr+Ba, respectively, and excess Si is 1.811 apfu (excess $Si = (Si^{4+} + Ti^{4+}) - (Al^{3+} + Fe^{3+} + Cr^{3+}) - 3*(Fe^{2+} + Mg^{2+} + Mn^{2+})$: equation 2 of Henderson and Oliveira, 2022). Therefore, $\square^{Si}$ and $\square^{Ca}$ are 0.906 apfu and 0.480 apfu, respectively, giving a total cavity cation-site vacancy of 1.386. Finally, following the calculation method of Henderson and Oliveira (2022), the chemical formula of the highest-Ca nepheline in the Kajishiyama basanite could be written as $(Ca_{0.467}Ba_{0.013}Na_{5.286}K_{0.919}\square^{Total}_{1.386})_{\Sigma 8.071}(Si_{0.912}Al_{6.980}Cr^{3+}_{0.003}Fe^{3+}_{0.067}Mg_{0.017})_{\Sigma 7.979}Si_{8.000}O_{32}$, i.e. $Ne_{65.50}Ks_{11.39}Q^{xs}_{11.22}CaNe_{11.89}$, where $\square^{Total}$ is the sum of $\square^{Si}$ and $\square^{Ca}$. Henderson and Oliveira (2022) and Oliveira and Henderson (2022) reported that K-rich nepheline and kalsilite have a trend including relatively high Mg and Fe^{2+} and showed a way to estimate the Fe^{2+} proportion in total Fe using the variation of the ΔAl^{cc} (change in *T* charge minus cavity cation charge: $T^{3+} + 2T^{2+} - M^{+} - 2M^{2+}$) and ΔT^{ch} (total analysed *T* charge minus charge for 16*T*: $4T^{4+} + 3T^{3+} + 2T^{2+} - 16*$mean *T* charge) stoichiometry parameters. In this study, however, we treated all iron as Fe^{3+} because the nepheline of Kajishiyama is low in Mg and Fe, and has a high Na/K ratio.

Formation process of the Ca-bearing nepheline in the basanite

We examined the process of fractionation of Kajishiyama basanites in order to consider the crystallisation conditions of nepheline. Miyashiro (1978) indicated that three different trends of differentiation appear to exist in large-scale alkalic volcanic association: 'Kennedy trend'; 'Coombs trend'; and the 'straddle type'. The 'Kennedy trend' is the trend away from the low-pressure thermal divide, which is defined by the Di–Ol–Pl plane in the model basalt Di–Ol–Ne–Qz tetrahedron (Yoder and Tilley, 1952), towards an increasing degree of undersaturation; thus, normative nepheline increases with fractionation. The 'Coombs trend' is the alkali trend that leads to peralkaline felsic rock; therefore, normative hypersthene increases with fractionation. The 'straddle type' shows composition ranges straddling the low-pressure thermal divide; therefore, normative nepheline decreases, followed by an increase in normative hypersthene with fractionation, ultimately towards Qz-normative compositions.

Figure 5a clearly indicates that nepheline is Ca-rich in basanite. The variations of normative plagioclase (anorthite + albite), normative nepheline and An/Ab ratio of normative plagioclase with fractionation are shown in Fig. 7 for the basanite sample set considered including the coeval Kajishiyama samples. Although there is a substantial amount of scatter, there appears to be a trend for total normative plagioclase to increase (Fig. 7a) and normative nepheline to decrease exponentially (Fig. 7b) in basanite with progress in magmatic fractionation in terms of increasing FeO (total iron)/MgO. Such a trend might be equivalent to the 'straddle type' of Miyashiro (1978), suggesting that the melt becomes enriched in Ca and silica due to crystallisation of low silica minerals, such as olivine, amphibole and magnetite (Miyashiro, 1978). The crystallisation sequence of the Kajishiyama basanite based on our petrographic observation is: (1) early phenocrysts and microphenocrysts of olivine and subordinate clinopyroxene, and their ulvöspinel inclusions; (2) later-formed plagioclase, alkali feldspar and apatite as groundmass; and (3) nepheline in mesostasis. This sequence is consistent with the character of crystallisation of 'straddle type' magma reported by Miyashiro (1978).

Nepheline is crystallised at the final stage of basanite solidification, and because Ca remains in the melt at that time, nepheline incorporates it and becomes enriched in Ca. The Ca content of nepheline is possibly controlled both by the Ca content of original magma and by the crystallising order of minerals, especially the timing of nepheline precipitation. Regarding the Kajishiyama basanite, if the magma is capable of nepheline crystallisation after precipitation of Na-rich plagioclase and alkali feldspar, the nepheline is possibly Ca-rich because of a relatively high Ca/Na ratio in the residual magma. The Kajishiyama basanites contain a small amount of calcite in druse (this study) as well as in the groundmass (Hirai and Arai, 1983), which means the deuteric fluid responsible for hydrothermal alteration after nepheline crystallisation was rich in Ca.

Factors controlling the Ca content of the nepheline in silica-undersaturated rocks

Even if the CaO content of the silica-undersaturated magma is the same as that of the basanite magma, the CaO content of the nepheline crystallising from it will make a difference. Most nephelinites contain Ca-poor nepheline in contrast to the Ca-rich nepheline of basanites (Fig. 5b). Some nephelinites, however, contain remarkably Ca-rich nepheline, such as basanitic nephelinites of the House Mountain volcano, Arizona, USA. (Wittke and Holm, 1996). What are the factors controlling the Ca content of the nepheline?

Melilite commonly occurs in the nephelinites, for example, the melilite–olivine nephelinite from Hamada, Japan (Tatsumi *et al.*, 1999, Hamada, 2011), olivine melilite nephelinite from Moiliili, Hawaii (Wilkinson and Stolz, 1983) and wollastonite nephelinite from Oldoinyo Lengai, Tanzania (Sharygin *et al.*, 2012) (Table 3). In fact, the CaO content of nephelines from these nephelinites is up to 0.34 wt.% (Hamada, 2011), 0.27 wt.% (Wilkinson and Stolz, 1983) and up to 0.46 wt.% (Sharygin *et al.*, 2012), respectively, and they are all Ca-poor.

https://doi.org/10.1180/mgm.2023.32 Published online by Cambridge University Press

It is considered that the removal of CaO from magma by the crystallisation of melilite, which is characterised by a high CaO content prior to, or simultaneously with, nepheline plays an important role in the crystallisation of Ca-poor nepheline. The nephelines from nephelinites without melilite, such as those from Nemby, eastern Paraguay (Comin-Chiaramonti *et al.*, 1991) and from House Mountain volcano (Wittke and Holm, 1996), are actually rich in Ca. In these basanites, the magma is high in CaO but not silica-undersaturated enough to crystallise melilite, thus Ca-rich nepheline crystallises.

Summary and implications

The Kajishiyama basanite is composed of olivine and augite as phenocrysts and microphenocrysts, and Ca-bearing nepheline, olivine, augite, ulvöspinel, plagioclase, alkali feldspar, apatite and zeolite in the groundmass. Basanites are of the 'straddle type' of Miyashiro (1978), indicating that normative plagioclase increases and normative nepheline decreases as fractionation progresses, where nepheline is precipitated at the last stage of solidification. Nepheline is possibly Ca-rich in the case of crystallisation from a high-normative plagioclase magma such as the Kajishiyama basanites. The occurrence of calcite in the druse indicates that the magma, which crystallised nepheline and the deuteric fluid were rich in Ca. Precipitation of melilite, which is highly Ca-rich, causes the low-Ca character of subsequently crystallising nepheline. For example, as shown in Fig. 5b, there are some reports of the presence of Ca-rich nepheline in nephelinites, which show no signature of melilite precipitation.

Acknowledgements. We thank Dr. Akihiro Tamura for his help during LA–ICP–MS measurements, Dr. Terumi Ejima of Shinshu University for her assistance in sample collection, Prof. Masayuki Okuno and Dr. Hiroki Okudera of Kanazawa University and Prof. Masahide Akasaka of Shimane University for their comments, advice and stimulating discussions, and three anonymous reviewers. Editors Roger Mitchell, Ian Coulson and Helen Kerbey are thanked for editorial assistance.

Competing interests. There are no conflicts of interest to declare.

References

Allen Jr. R.O., Zweifel K., Haskin L.A. and Marvin U.B. (1970) Simultaneous analysis for 38 elements in chips and separated phases of the Bruderheim chondrite. *Meteoritics*, **5**, 179.

Antao S.M. and Hassan I. (2010) Nepheline: Structure of three samples from the Bancroft area, Ontario, obtained using synchrotron high-resolution powder X-ray diffraction. *The Canadian Mineralogist*, **48**, 69–80.

Antao S.M. and Nicholls J.W. (2018) Crystal chemistry of three volcanic K-rich nepheline samples from Oldoinyo Lengai, Tanzania and Mount Nyiragongo, Eastern Congo, Africa. *Frontiers in Earth Science*, **6**, 155.

Balassone G., Kahlenberg V., Altomare A., Mormone A., Rizzi R., Saviano M. and Mondillo N. (2014) Nephelines from the Somma-Vesuvius volcanic complex (Southern Italy): crystal-chemical, structural and genetic investigations. *Mineralogy and Petrology*, **108**, 71–90.

Blancher S.B., D'arco P., Fonteilles M. and Pascal M.L. (2010) Evolution of nepheline from mafic to highly differentiated members of the alkaline series: the Messum complex, Namibia. *Mineralogical Magazine*, **74**, 415–432.

Brown F.H. and Carmichael I.S.E. (1969) Quaternary volcanoes of the Lake Rudolf Region: 1. The basanite-tephrite series of the Korath Range. *Lithos*, **2**, 239–260.

Buerger M.J. (1954) The stuffed derivatives of the silica structures. *American Mineralogist*, **39**, 600–614.

Comin-Chiaramonti P., Civetta L., Petrini R., Piccirillo E.M., Bellieni G., Censi P., Bitschene P., Demarchi. G., De Min A., Gomes C.B., Castillo A.M. and Velazquez J.C. (1991) Tertiary nephelinitic magmatism in Eastern Paraguay: petrology, Sr-Nd isotopes and genetic relationships with associated spinel-peridotite xenoliths. *European Journal of Mineralogy*, **3**, 507–525.

Dawson J.B. (1998) Peralkaline nephelinite-natrocarbonatite relationships at Oldoinyo Lengai, Tanzania. *Journal of Petrology*, **39**, 2077–2094.

Deer W.A., Howie R.A. and Zussman J. (1963) *Rock-forming Minerals: Vol. 4: Framework Silicates*. Longman, UK.

Dollase W.A. (1970) Least-squares refinement of the structure of a plutonic nepheline. *Zeitschrift für Kristallographie – Crystalline Materials*, **132**, 27–44.

Dollase W.A. and Thomas W.M. (1978) The crystal chemistry of silica-rich, alkali-deficient nepheline. *Contributions to Mineralogy and Petrology*, **66**, 311–318.

Donnay G., Schairer J.F. and Donnay J.D.H. (1959) Nepheline solid solutions. *Mineralogical magazine and journal of the Mineralogical Society*, **32**, 93–109.

Foreman N. and Peacor D.R. (1970) Refinement of the nepheline structure at several temperatures. *Zeitschrift für Kristallographie – Crystalline Materials*, **132**, 45–70.

Garcia M.O., Frey F.A. and Grooms D.G. (1986) Petrology of volcanic rocks from Kaula Island, Hawaii. *Contributions to Mineralogy and Petrology*, **94**, 461–471.

Gibson S.A., Thompson R.N., Leonardos O.H. Dickin A.P. and Mitchell J.G. (1999) The limited extent of plume-lithosphere interactions during continental flood-basalt genesis: geochemical evidence from Cretaceous magmatism in southern Brazil. *Contributions to Mineralogy and Petrology*, **137**, 147–169.

Goto K. and Arai S. (1986) Nepheline basanite from Nanzaki volcano, Izu Peninsula, central Japan. *Journal of Geological Society of Japan*, **92**, 307–310.

Hahn T. and Buerger M.J. (1955) The detailed structure of nepheline, $KNa_3Al_4Si_4O_{16}$. *Zeitschrift für Kristallographie – Crystalline Materials*, **106**, 308–338.

Hamada M. (2011) Sr-Na-bearing åkermanite and nepheline in nephelinite from Nagahama, Hamada, Shimane prefecture, southwest Japan. *Journal of Mineralogical and Petrological Sciences*, **106**, 187–194.

Hamada M., Akasaka M. and Ohfuji H. (2019) Crystal chemistry of K-rich nepheline in nephelinite from Hamada, Shimane Prefecture, Japan. *Mineralogical Magazine*, **83**, 239–247.

Hassan I., Antao S.M. and Hersi A.A. (2003) Single-crystal XRD, TEM, and thermal studies of the satellite reflections in nepheline. *The Canadian Mineralogist*, **41**, 759–783.

Henderson C.M.B. (2020) Nepheline solid solution compositions: stoichiometry revisited, reviewed, clarified and rationalized. *Mineralogical Magazine*, **84**, 813–838.

Henderson C.M.B. and de Oliveira Í.L. (2022) Substitution of 'small' divalent cations (e.g. Mg) for Si and Al in the nepheline tetrahedral framework: 1. Calculation of atomic formulae and stoichiometry parameters. *Mineralogical Magazine*, **86**, 243–253.

Henderson C.M.B. and Gibb F.G.F. (1972) Plagioclase-Ca-rich-nepheline intergrowths in a syenite from the Marangudzi complex, Rhodesia. *Mineralogical Magazine*, **38**, 670–677.

Henderson C.M.B. and Gibb F.G.F. (1983) Felsic mineral crystallisation trends in differentiating alkaline basic magmas. *Contributions to Mineralogy and Petrology*, **84**, 355–364.

Henderson C.M.B. and Taylor D. (1982) The structural behaviour of the nepheline family: 1. Sr and Ba aluminates (MAl_2O_4), *Mineralogical Magazine*, **45**, 111–127.

Hirai H. and Arai S. (1983) Finding of nepheline in some alkali basalts from southwest Japan. *Journal of the Geological Society of Japan*, **89**, 531–534.

Hirai H. and Arai S. (1986) Formation of analcime and phillipsite in hydrous basanites from Southwestern Japan. *Neues Jahrbuch für Mineralogie. Abhandlungen*, **153**, 163–176.

Ikeda Y. (1980) Petrology of Allan Hills-764 Chondrites (LL3). *Memoirs of National Institute of Polar Research., Special issue*, **17**, 50–82.

Iwamori H. (1991) Zonal structure of Cenozoic basalts related to mantle upwelling in southwest Japan. *Journal of Geophysical Research: Solid Earth*, **96**(B4), 6157–6170.

Kimura M. and Ikeda Y. (1995) Anhydrous alteration of Allende chondrules in the solar nebula II: Alkali-Ca exchange reactions and formation of nepheline, sodalite and Ca-rich phases in chondrules. *Antarctic Meteorite Research*, **8**, 123.

Kimura J.I., Stern R.J. and Yoshida T. (2005a) Reinitiation of subduction and magmatic responses in SW Japan during Neogene time. *Geological Society of America Bulletin*, **117**, 969–986.

https://doi.org/10.1180/mgm.2023.32 Published online by Cambridge University Press

Le Bas M.J. (1989) Nephelinitic and basanitic rocks. *Journal of Petrology*, **30**, 1299–1312.

Miyashiro A. (1978) Nature of alkalic volcanic rock series. *Contributions to Mineralogy and Petrology*, **66**, 91–104.

Nakamura E., McDougall I. and Campbell I.H. (1986) K-Ar ages for basalts from the Higashi-Matsuura district, northwestern Kyushu, Japan and regional geochronology of the Cenozoic alkaline volcanic rocks in eastern Asia. *Geochemical Journal*, **20**, 91–99.

Nguyen T.T., Kitagawa H., Pineda-Velasco I. and Nakamura E. (2020) Feedback of slab distortion on volcanic arc evolution: Geochemical perspective from late Cenozoic volcanism in SW Japan. *Journal of Geophysical Research: Solid Earth*, **125**, e2019JB019143.

Oliveira Í.L. and Henderson C.M.B. (2022) Substitution of 'small' divalent cations (e.g. Mg) for Si and Al in the nepheline tetrahedral framework: 2. The occurrence of Mg-rich nepheline and kalsilite. *Mineralogical Magazine*, **86**, 254–262.

Oshika J., Arakawa Y., Endo D., Shinmura T. and Mori Y. (2014) A rare basanite distribution in the northern part of the Izu–Bonin volcanic arc, Japan: Petrological and geochemical constraints. *Journal of Volcanology and Geothermal Research*, **270**, 76–89.

Paslick C.R., Halliday A.N., Lange R.A., James D. and Dawson J.B. (1996) Indirect crustal contamination: evidence from isotopic and chemical disequilibria in minerals from alkali basalts and nephelinites from northern Tanzania. *Contributions to Mineralogy and Petrology*, **125**, 277–292.

Perepelov A.B., Puzankov M.Y., Ivanov A.V., Filosofova T.M., Demonterova E.I., Smirnova E.V., Chuvashove L.A. and Yasnygina T.A. (2007) Neogene basanites in western Kamchatka: mineralogy, geochemistry, and geodynamic setting. *Petrology*, **15**, 488–508.

Peterson T.D. (1989) Peralkaline nephelinites. I. Comparative petrology of Shombole and Oldoinyo L'engai, East Africa. *Contributions to Mineralogy and Petrology*, **101**, 458–478.

Roedder E.W. (1951) The system K_2O–MgO–SiO_2. *American Journal of Science*, **249**, 81–130 and 224–248.

Roedder E. (1952) A reconnaissance of the liquidus relationships in the system $K_2O{\cdot}2SiO_2$–FeO–SiO_2. *American Journal of Science,* (*Bowen volume*), **250A**, 435–456.

Roedder E. (1978) Silicate liquid immiscibility in magmas and in the system K_2O–FeO–Al_2O_3–SiO_2: an example of serendipity. *Geochimica et Cosmochimica Acta*, **42**, 1597–1617.

Sahama T.G. and Wiik H.B. (1952) Leucite, potash nepheline, and clinopyroxene from volcanic lavas from southwestern Uganda and adjoining Belgian Congo. *American Journal of Science*, **250**, 457–470.

Sharygin V.V., Kamenetsky V.S., Zaitsev A.N. and Kamenetsky M.B. (2012) Silicate–natrocarbonatite liquid immiscibility in 1917 eruption combeite–wollastonite nephelinite, Oldoinyo Lengai Volcano, Tanzania: Melt inclusion study. *Lithos*, **152**, 23–39.

Simmons Jr., W.B. and Peacor D.R. (1972) Refinement of the crystal structure of a volcanic nepheline. *American Mineralogist: Journal of Earth and Planetary Materials*, **57**, 1711–1719.

Sun S.S. and McDonough W.F. (1989) Chemical and isotopic systematics of oceanic basalts: implications for mantle compositions and processes. *Geological Society, London, Special Publications*, **42**, 313–345.

Tait K.T., Sokolova E. and Hawthorne F.C. (2003) The crystal chemistry of nepheline. *The Canadian Mineralogist*, **41**, 61–70.

Takamura H. (1973) Petrographical and petrochemical studies of the Cenozoic basaltic rocks in Chugoku province. *Geological Reports of Hiroshima University*, **18**, 1–167.

Tatsumi Y., Arai R. and Ishizaka K. (1999) The petrology of a melilite-olivine nephelinite from Hamada, SW Japan. *Journal of Petrology*, **40**, 497–509.

Uto K., Hirai H. and Arai S (1986) K-Ar ages of some ultramafic xenolith-bearing alkali basalts in southwestern Japan. *Abstracts of Annual Joint Meeting of the Japanese Association of Petrologists, Mineralogists and Economic Geologists, the Mineralogical Society of Japan and the Society of Mining Geology of Japan*, **115**.

Vulić P., Balić-Žunić T., Belmonte L.J. and Kahlenberg V. (2011) Crystal chemistry of nephelines from ijolites and nepheline-rich pegmatites: influence of composition and genesis on the crystal structure investigated by X-ray diffraction. *Mineralogy and Petrology*, **101**, 185–194.

Wilkinson J.F.G. and Hensel H.D. (1994) Nephelines and analcimes in some alkaline igneous rocks. *Contributions to Mineralogy and Petrology*, **118**, 79–91.

Wilkinson J.F.G. and Stolz A.J. (1983) Low-pressure fractionation of strongly undersaturated alkaline ultrabasic magma: the Olivine-Melilite-Nephelinite at Moiliili, Oahu, Hawaii. *Contributions to Mineralogy and Petrology*, **83**, 363–374.

Wittke J.H. and Holm R.F. (1996) The association basanitic nephelinite; feldspar ijolite-nepheline monzosyenite at House Mountain Volcano, north-central Arizona. *The Canadian Mineralogist*, **34**, 221–240.

Zaitsev A.N., Marks M.A.W., Wenzel T., Spratt J., Sharygin V.V., Strekopytov S. and Markl G. (2012) Mineralogy, geochemistry and petrology of the phonolitic to nephelinitic Sadiman volcano, Crater Highlands, Tanzania. *Lithos*, **152**, 66–83.

https://doi.org/10.1180/mgm.2023.32 Published online by Cambridge University Press